

## Supporting Information

### Boosting Water Oxidation on Cu<sub>2</sub>V<sub>2</sub>O<sub>7</sub> by Atomic-Scale Frustrated Lewis Pairs

Zheng-Yi Huang,<sup>a</sup> Bowen Liao,<sup>a, c</sup> Xiaoxuan Song,<sup>a</sup> San Ping Jiang,<sup>b</sup> Xiaoxia Li,<sup>c</sup> Shuwang Duo,<sup>\*a</sup> Zhong Chen,<sup>\*a</sup> Jingwei Li<sup>\*b</sup>

a: Jiangxi Province Key Laboratory of Surface Engineering, School of Materials and Energy, Jiangxi Science and Technology Normal University, Nanchang 330013, China

b: National Energy Key Laboratory for New Hydrogen-Ammonia Energy Technologies, Foshan Xianhu Laboratory, Foshan 528216, China

c: Institute of Functional Materials, Jiangxi University of Finance and Economics, Nanchang 330013, PR China

## Structure characterization

The phase composition of the samples is detected by X-ray diffraction (XRD, Cu K $\alpha$  radiation,  $\lambda = 0.154$  nm). The morphology and lattice structure of the samples were examined by Field emission scanning electron microscopy (FE-SEM, EISS-SIGMA HD, 15 kV, 1nA) and Transmission electron microscopy (TEM, JEOL F200, 100kV, 2.5 nA). Spherical aberration corrected Transmission Electron Microscope (AC-TEM, Thermo Scientific Themis Z, 200kV) is used to characterize the atomic arrangements on the surface of samples (USA-FEI-Titan Cubed Themis G2 300). The sample composition was determined by X-ray Photoelectron Spectroscopy (XPS, ThermoFisher Nexsa). Raman spectra (Raman, Renishaw inVia) are used to characterize the molecular structure and chemical bonding of catalysts.

## Optica characterization

UV-Visible (UV-Vis) absorption spectra were recorded by UV-Vis-NIR (Shimadzu UV 3600 Plus, 280~800 nm) spectrophotometer. The irradiative recombination of electrons and holes of all samples was evaluated by photoluminescence spectroscopy (PL, Edinburgh FLS 1000, excitation wavelength: 365 nm) and Time resolved photoluminescence spectroscopy (TRPL, Edinburgh FLS 1000, excitation wavelength: 365 nm) to investigate the charge separation process.

## Computational details

Based on the XRD and TEM information, CVO (200) and crystal faces were selected to construct the model. Spin-polarized electronic structure calculations were performed using the plane-wave basis set approach as implemented in the Vienna ab initio simulation package (VASP).<sup>1</sup> The projector augmented wave (PAW) method was used to represent the ion–core electron interactions.<sup>2</sup> The valence electrons were represented with a plane wave basis set with an energy cutoff of 450 eV. Electronic exchange and correlation were described with the Perdew–Burke–Ernzerhof (PBE) functional.<sup>3</sup> DFT-D3 method was used to treat the van der Waals interaction.<sup>4</sup> A  $2 \times 2 \times 1$  Monkhorst–Pack scheme was used to generate the k-point grid for the modeled surfaces.<sup>5</sup> The convergence criteria for the self-consistent electronic structure and geometry were set to 10–5 eV and 0.05 eV/Å, respectively. Molecular dynamics (MD) simulations were conducted using the Force module with the COMPASS force field in Materials Studio.<sup>6</sup> Van der Waals and Coulomb interactions were considered, using atom-based and Ewald methods with a 12.5 Å cutoff. The motion equations were integrated at a 1 fs time step. Following energy

minimization, each system underwent a 500 ps relaxation period under periodic boundary conditions in the NVT ensemble, using the Nose thermostat and Berendsen barostat for stabilization of temperature, potential, and total energy.

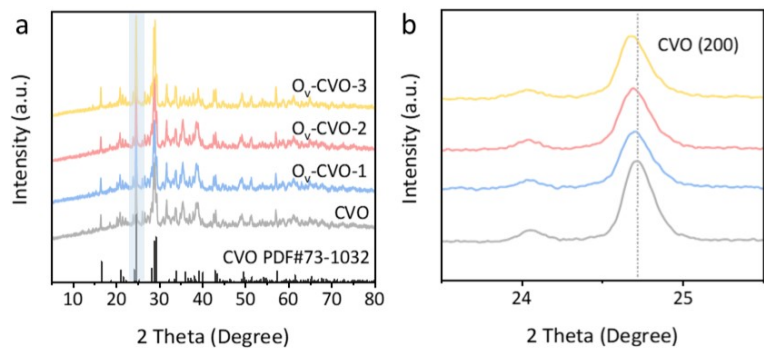


**Fig. S1.** XRD patterns of CVO, Vo-CVO-1, O<sub>v</sub>-CVO-2 and O<sub>v</sub>-CVO-3. (a) Total XRD patterns. (b) Locally amplified XRD patterns.

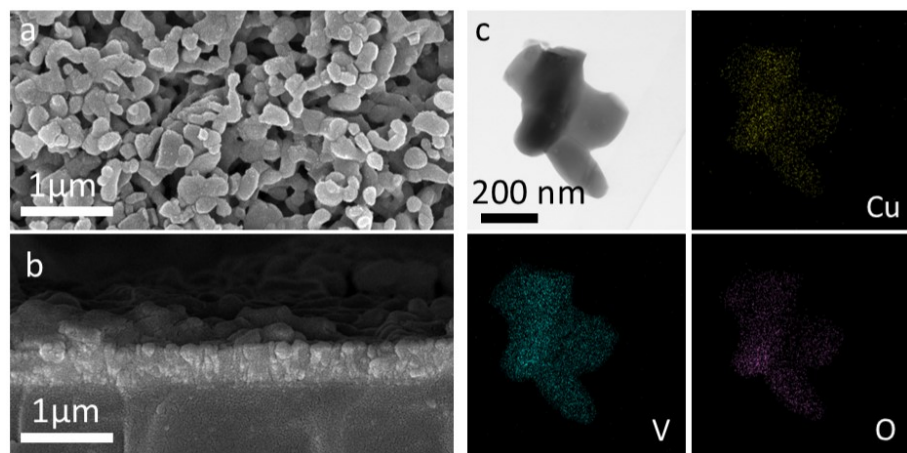


**Fig. S2.** (a) Longitudinal SEM images of CVO. (b) Transverse SEM images of CVO. (c) Mapping images of CVO.

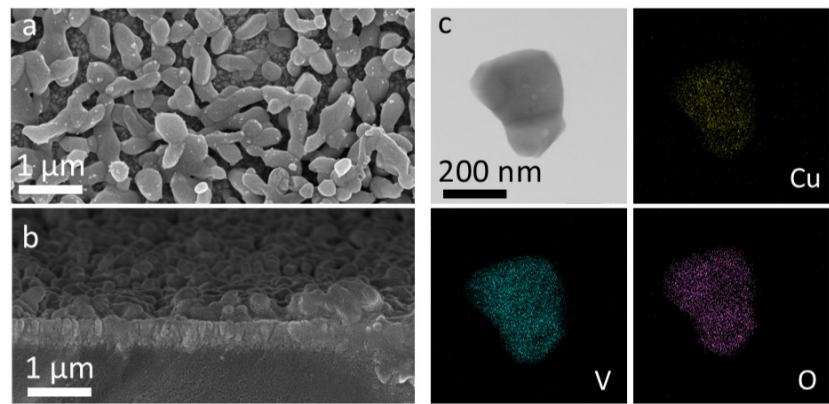


**Fig. S3.** (a) Longitudinal SEM images of O<sub>v</sub>-CVO-2. (b) Transverse SEM images of O<sub>v</sub>-CVO-2. (c) Mapping images of O<sub>v</sub>-CVO-2

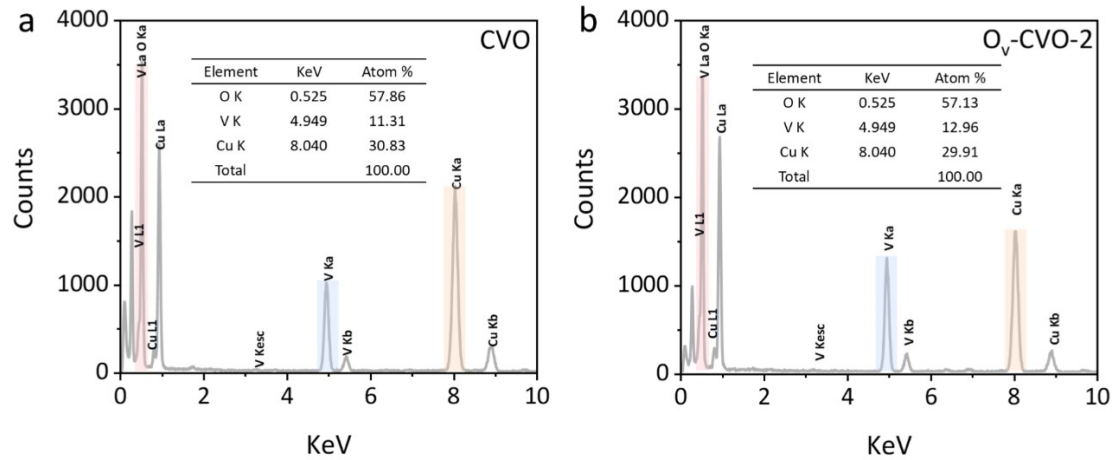


**Fig. S4.** (a) Energy dispersive spectrometer of CVO (b) Energy dispersive spectrometer of O<sub>v</sub>-CVO-2.

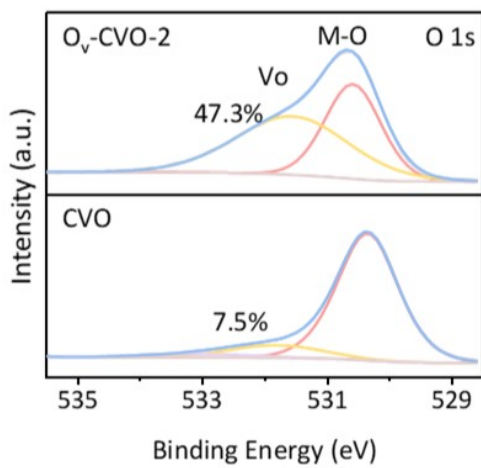


**Fig. S5.** O 1s curves of CVO and  $O_v$ -CVO-2.

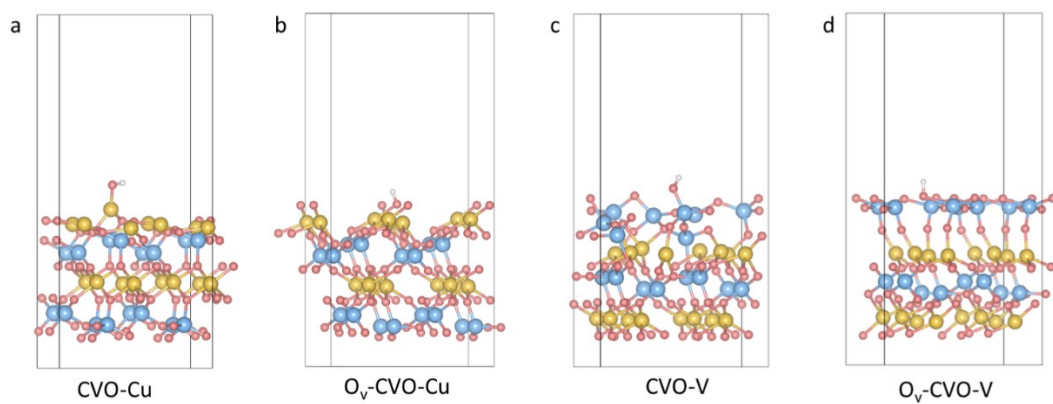


**Fig. S6.** The structure for calculating the adsorption energy of -OH by CVO and  $O_v$ -CVO. (a) CVO-Cu site. (b)  $O_v$ -CVO-Cu site. (c) CVO-V site. (d)  $O_v$ -CVO-V site.

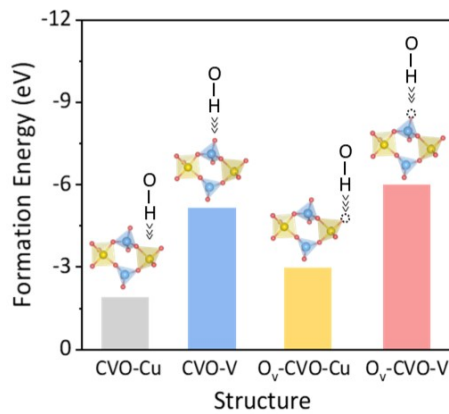


**Fig. S7.** Adsorption energy of CVO and  $O_v$ -CVO-2 at different sites.

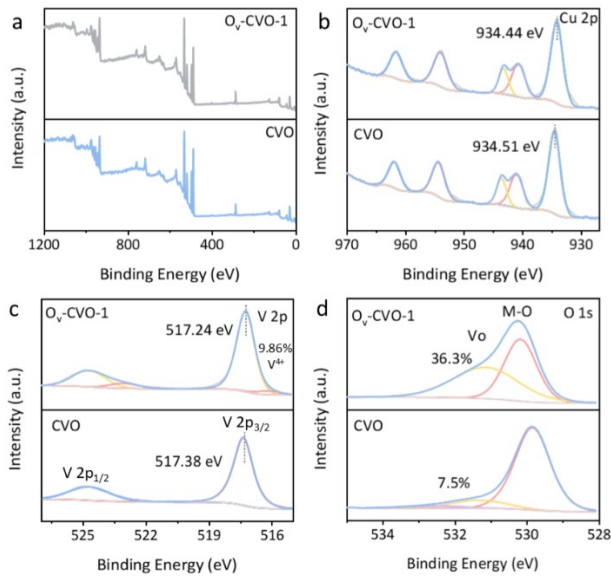


**Fig. S8.** XPS patterns of CVO and  $O_v$ -CVO-1. (a) Full curves. (b) Cu 2p curves. (c) V 2p curves. (d) O 1s curves.

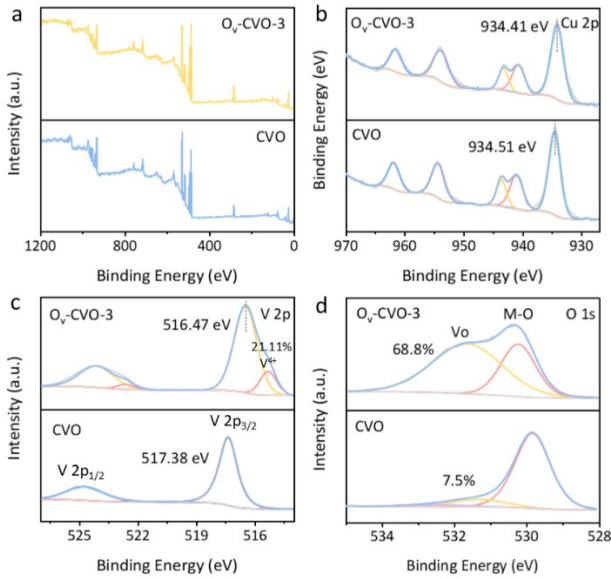


**Fig. S9.** XPS patterns of CVO and  $O_v$ -CVO-3. (a) Full curves. (b) Cu 2p curves. (c) V 2p curves. (d) O 1s curves.

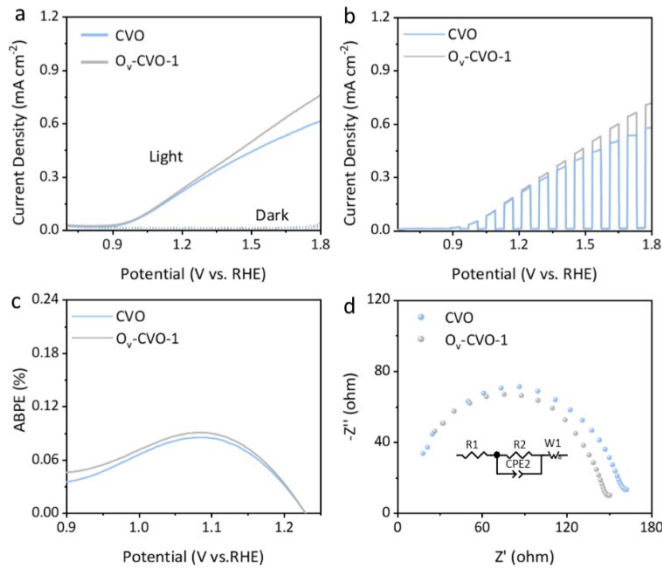


**Fig. S10.** The electrochemical test curve of CVO and  $O_v$ -CVO-1. (a) LSV curve. (b) LSV curve under chopping light. (c) ABPE curve; (d) EIS plots.

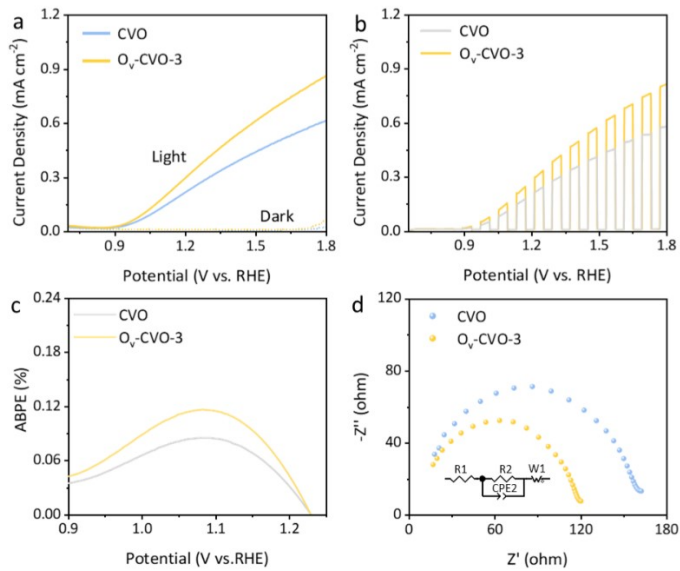


**Fig. S11.** The electrochemical test curve of CVO and  $O_v$ -CVO-3. (a) LSV curve. (b) LSV curve under chopping light. (c) ABPE curve; (d) EIS plots.

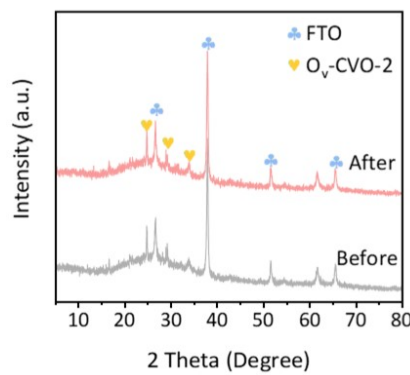


**Fig. S12.** XRD patterns of O<sub>v</sub>-CVO-2 before and after stability tests.

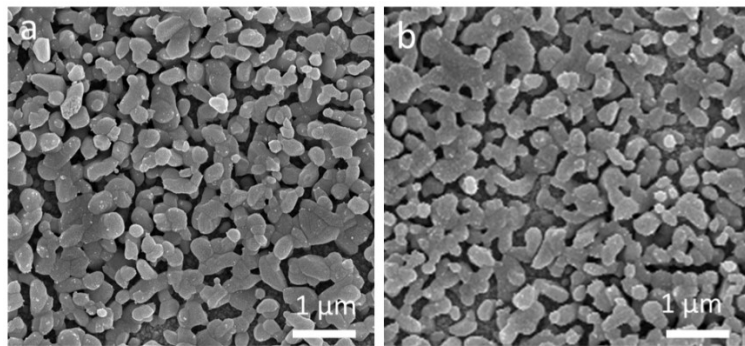


**Fig. S13.** SEM images before and after the stability test of O<sub>v</sub>-CVO-2. (a) SEM image before reaction. (b) SEM image after the reaction.

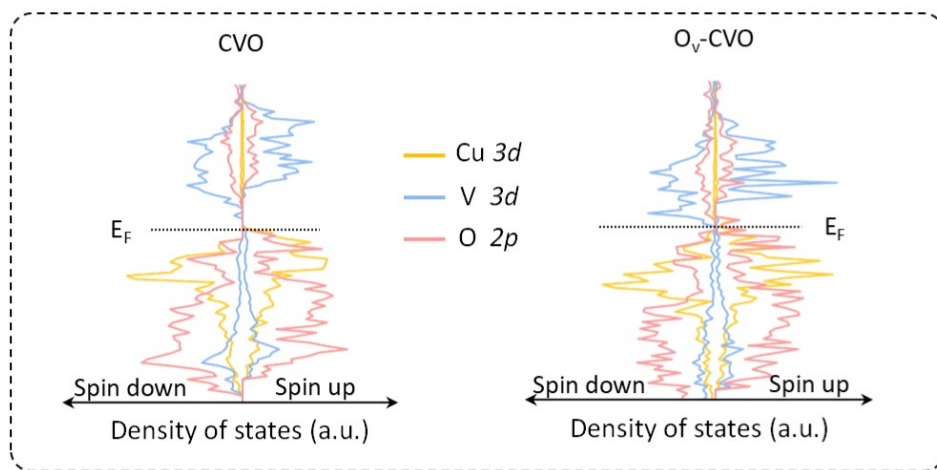


**Fig. S14.** PDOS of CVO and O<sub>v</sub>-CVO.

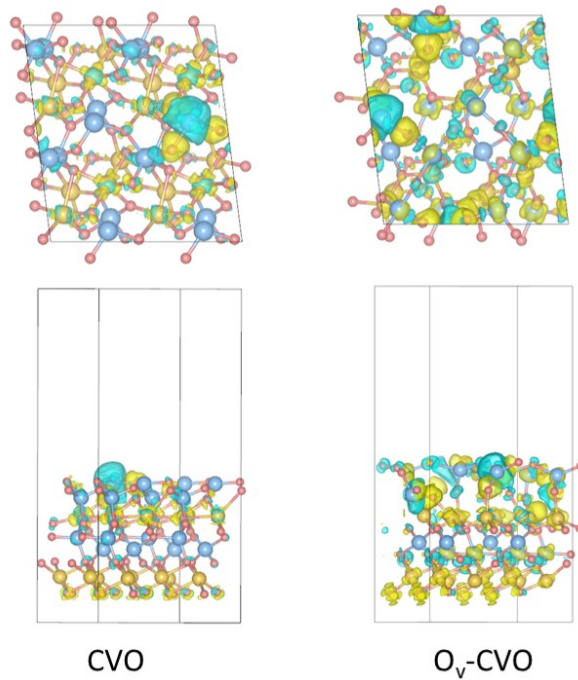


**Fig. S15.** The differential charge structure models of CVO and O<sub>v</sub>-CVO.

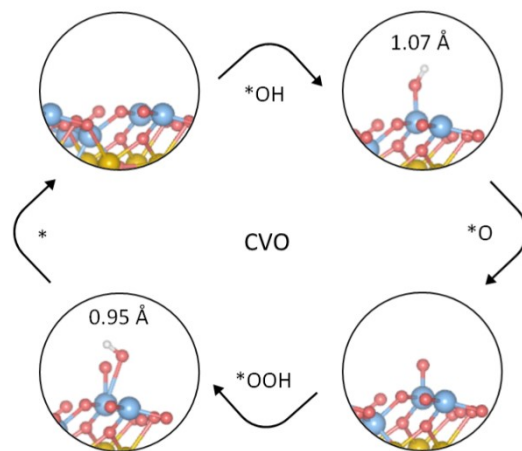


**Fig. S16.** Adsorption model of CVO in the OER process and O-H bond length.

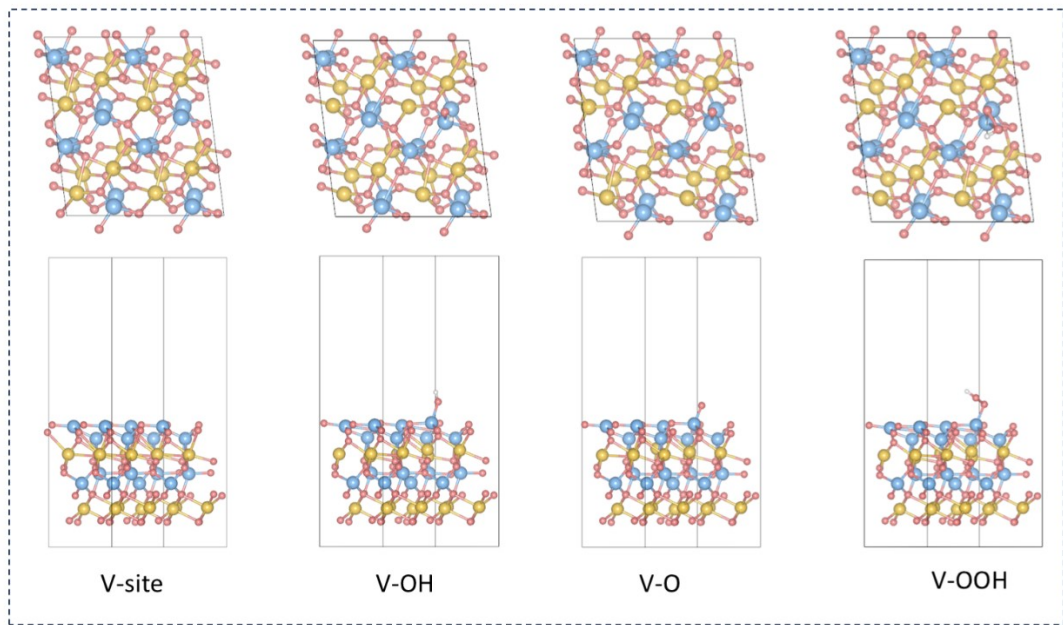


**Fig. S17.** The structural type of the OER intermediate on CVO.

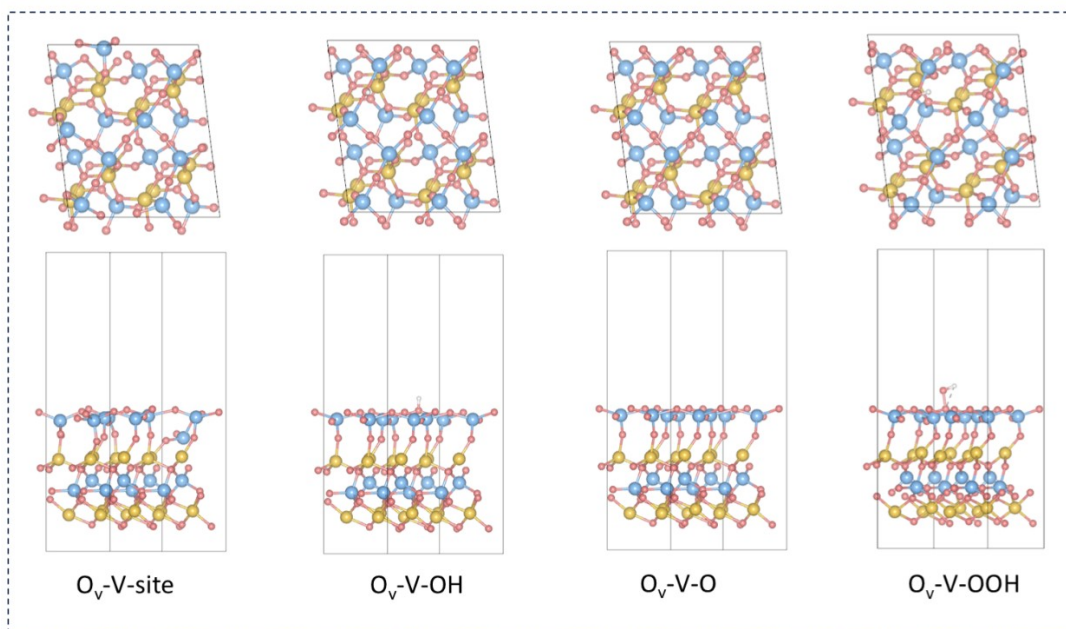


**Fig. S18.** The structural type of the OER intermediate on O<sub>v</sub>-CVO.

**Table S1.** Equivalent circuit fitting parameters of EIS curves for CVO, O<sub>v</sub>-CVO-1, O<sub>v</sub> -CVO-2 and O<sub>v</sub> -CVO-3.

	CVO	O <sub>v</sub> -CVO-1	O <sub>v</sub> -CVO-2	O <sub>v</sub> -CVO-3
R <sub>s</sub> (Ω)	11.28	7.61	6.34	6.94
R <sub>ct</sub> (Ω)	94.97	73.96	51.79	52.63

## Reference:

- [1] G. Kresse and J. Furthmüller, *Computational materials science*, 1996, **6**, 15-50.
- [2] G. Kresse and D. Joubert, *Physical review b*, 1999, **59**, 1758.
- [3] J. P. Perdew, K. Burke and M. Ernzerhof, *Physical review letters*, 1996, **77**, 3865.
- [4] S. Grimme, J. Antony, S. Ehrlich and H. Krieg, *The Journal of chemical physics*, 2010, **132**, 154104.
- [5] H. J. Monkhorst and J. D. Pack, *Physical review B*, 1976, **13**, 5188.
- [6] H. Sun, *The Journal of Physical Chemistry B*, 1998, **102**, 7338-7364.